




# A Photometric Analysis of the Relationship between the UV flux of Type Ia Supernovae and Host-galaxy Metallicity

Peter J. Brown<sup>1,2</sup>  and Nicole R. Crumpler<sup>1,3</sup>

<sup>1</sup> Department of Physics and Astronomy, Texas A&M University, 4242 TAMU, College Station, TX 77843, USA; [pbrown@physics.tamu.edu](mailto:pbrown@physics.tamu.edu)

<sup>2</sup> George P. and Cynthia Woods Mitchell Institute for Fundamental Physics & Astronomy, USA

<sup>3</sup> Department of Physics, Duke University, Durham, NC 27708, USA

Received 2019 September 11; revised 2019 December 2; accepted 2019 December 30; published 2020 February 11

## Abstract

The effect of progenitor metallicity on Type Ia supernovae (SNe Ia) has important cosmological implications due to the need for these standardizable candles to be compared across large spans of cosmic time in which the progenitor stars might have different properties. Theoretical models have come to different conclusions as to the wavelength range impacted by metallicity differences, leading to differing interpretations of the growing sample of UV observations. Recent work has claimed a correlation between the mid-UV flux of SNe Ia measured from *Swift* grism spectra and the gas-phase metallicities measured for their host galaxies. Here we examine UV photometry for the same objects. We find no significant correlations between the UV–optical colors (or UV/optical count rate ratios) of the SNe Ia and the host-galaxy properties of mass or metallicity. The lack of a significant correlation with host-galaxy metallicity implies that a physical difference other than progenitor metallicity dominates the UV flux differences. Understanding the existing observations requires improved theoretical models and a larger parameter space of physical differences.

*Unified Astronomy Thesaurus concepts:* Type Ia supernovae (1728); Metallicity (1031)

## 1. Introduction

Type Ia supernovae (SNe Ia) are important cosmological tools because their similarly high luminosities allow them to be used as standard candles to measure distances. The dispersion in luminosities can be reduced with corrections for the light-curve shape and colors (Hamuy et al. 1996; Riess et al. 1996; Phillips et al. 1999). Correlations have also been found with host-galaxy mass (Kelly et al. 2010; Lampeitl et al. 2010; Childress et al. 2013; Hayden et al. 2013; Moreno-Raya et al. 2016) and are now corrected for in most cosmological studies (Scolnic et al. 2018). A variation in the magnitude of the so-called “mass step” has been found for different surveys, filter choices, and SN fitters (Kim et al. 2014; Brout et al. 2019). Correlations have also been found with the local host-galaxy parameters (Rigault et al. 2013; Galbany et al. 2014). The physical connection between the host-galaxy parameters and the SN luminosities is not yet clear. The concern is that systematic differences in the progenitors could change the observed properties of the explosion in a way not corrected for in the current methods of standardization.

Metallicity, here referring to the pre-explosion chemical abundances in the white dwarf, has been worried about as a potential systematic for many years (Höflich et al. 1998; Mazzali & Podsiadlowski 2006) because of the secular building-up of metals in the universe and the different chemical compositions of the galaxies hosting SNe Ia. Many models have explored how changes in progenitor metallicity will affect the bolometric and broadband fluxes of SNe Ia (Timmes et al. 2003, see also De et al. 2014 and references therein). Those which calculated effects at UV wavelengths found stronger effects in the UV than in the optical (Lentz et al. 2000; Sauer et al. 2008; Walker et al. 2012; Miles et al. 2016), though they differed from each other in how much or in what wavelength regions the effects are seen.

Foley & Kirshner (2013) presented UV spectra of two SNe Ia that are nearly identical twins in terms of near-UV/optical spectra and light-curve shapes. The most significant difference is in the mid-UV flux level. By comparison with the models of Lentz et al. (2000), they found that a relative metallicity difference could approximate the spectral changes in the mid-UV. Brown et al. (2015) found that the same metallicity differences could be inferred from broadband photometry from the *Neil Gehrels Swift Observatory*’s Ultra-Violet Optical Telescope (*Swift*/UVOT), given the assumption that the color variations were caused by the same metallicity differences as between the epoch 15 models of Lentz et al. (2000). Brown et al. (2015) also showed, however, that the UV flux levels of the models of Lentz et al. (2000) were too high and that even the relative color differences between objects did not match the multi-epoch color differences of SNe 2011by and 2011fe. Using a different set of models from Walker et al. (2012), Brown et al. (2019) found that SN 2011fe had UV flux levels comparable to low-metallicity models while the redder SN 2017erp featured a depressed UV continuum that matched the higher-metallicity models. From the observations, it is clear that significant but distinct variations appear in the mid-UV and near-UV (NUV) wavelength regions; however, the same physical difference—metallicity—has been invoked for both of the spectral ranges.

A promising approach is to look for other observables that correlate with the UV differences (e.g., Milne et al. 2013; Brown et al. 2018). Pan et al. (2020) report a correlation between the host-galaxy metallicity and  $f_{2535}$ , the ratio of the mid-UV flux between 2450 and 2620 Å to the optical flux between 4000 and 4500 Å, as measured in grism observations with *Swift*/UVOT (Gehrels et al. 2004; Roming et al. 2005; Kuin et al. 2015). In this article we report whether we can confirm such a correlation from the *Swift*/UVOT photometry of the same objects. As shown below, the photometry does not show a correlation with the host-galaxy properties.

## 2. Observations

The photometry used is from the *Swift* Optical Ultraviolet Supernova Archive (Brown et al. 2014). Most of the photometry has been previously published and made available via the *Swift* SN website<sup>4</sup> and the Open Supernova Catalogue (Guillochon et al. 2017), while four additional objects were reduced and added following the posting of Pan et al. (2020).

Some objects from Pan et al. (2020) are not included, because we do not yet have pre-explosion or late-time images from which to subtract the underlying galaxy contribution to the observed count rates. This turns out to be especially important for the sample used by Pan et al. (2020). SN 2016ccz has the lowest host-galaxy metallicity in their sample and is claimed to have the highest mid-UV/optical flux ratio. This object dominates the UV–metallicity relationship in Pan et al. (2020). In our photometry analysis, we do not significantly detect SN 2016ccz in the mid-UV *uvm2* filter after subtraction of the host-galaxy flux. While the UVOT grism reduction of Pan et al. (2018) has some improvements compared to the default extractions, it can only estimate the underlying contribution based on the background flux on either side of the source spectrum. It does not use the more accurate spectral template image subtraction as in Smitka et al. (2016). This is necessary in cases of strong, non-uniform galaxy contamination. In the case of SN 2016ccz, the mid-UV flux in their spectrum must be dominated by the galaxy. As SN 2016ccz is not detected significantly and has a negative count rate consistent with zero flux, it would be excluded or treated as an upper limit if fitting the magnitudes or colors. Instead, we use the count rates and count rate errors at the epoch closest to the time of *B*-band maximum light to test for correlations with the host-galaxy mass or metallicity.

We use the host-galaxy parameters as measured by Pan et al. (2020). They derived host-galaxy masses from fits to multi-color photometry. The host-galaxy metallicities are calculated from emission line measurements from optical spectra on the calibration of Pettini & Pagel (2004).

## 3. Analysis

We first confirm that the observed colors are similar to those of other UV photometric Ia samples studied previously (e.g., Brown et al. 2010, 2017; Milne et al. 2010, 2013). Figure 1 shows the evolution of SN Ia color plotted with color regions signifying NUV–blue and NUV–red SNe as designated by Milne et al. (2013). By fraction, the NUV–red SNe have previously been observed to be more common (Milne et al. 2013, 2015) at low redshift. This sample seems to have a larger fraction of NUV–blue SNe Ia. The spectroscopic nature of this sample could be biased, either in triggering or in publishing SNe Ia with higher (and thus more detectable) UV flux. The higher flux could result from intrinsic differences or from lower host-galaxy or Milky Way reddening. However, a similar range of colors is observed.

The plots of color evolution are not corrected for reddening, which can have the effect of shifting an NUV–blue SN Ia into the NUV–red parameter space (Brown et al. 2017). To account for reddening, Figure 2 displays the observed colors, but with a reddening track showing the effect of different reddening laws. The vertical dispersion is indicative of

intrinsic UV differences. Splitting the sample at  $12 + \log(\text{OH}) = 8.6$  based on the values given in Pan et al. (2020), we find that both groups disperse vertically, though the group with higher metallicity has a smaller spread in *B* – *V* color. Regardless of whether the NUV–blue/red groups are distinct or a continuous color parameter, they are not related to the host-galaxy metallicity.

We now look directly for correlations between the UV flux of this SN Ia sample and the properties of the host galaxies. To make a clearer comparison with the UV–optical flux ratios shown in Pan et al. (2020), we use the UVOT filter *uvm2* for the mid-UV, and *uvw1* and *u* for the near-UV, and *B* for the optical (sometimes designated as *b* as per the UVOT convention). To incorporate the undetected flux of SN 2016ccz we now use measured count rates and associated errors at the epoch closest to maximum light in the *B* band rather than the fitted magnitudes. We first correct the count rates for the estimated Milky Way reddening (Schlafly & Finkbeiner 2011) and the host-galaxy reddening using the values from Pan et al. (2020). Some of the host-galaxy reddening values of Pan et al. (2020) are actually from the galaxy spectral fitting and thus not necessarily reflective of the line-of-sight reddening to an SN in or near a particular part of the host galaxy. The results from fits of the colors corrected in this way are given in Table 1. Because the differences between the two reddening corrections do not show any significant correlations with host-galaxy mass or metallicity, they do not affect the conclusions. We make a separate correction assuming that all of the SNe Ia have the same *B* – *V* color at the time of maximum in the *B* band, set to the bluest object in this sample with  $(B - V)_{\text{Bpeak}} = -0.15$ . The count rates are corrected for reddening using the extinction coefficients derived from the reddening law of Cardelli et al. (1989) with  $R_V = 3.1$  and the SN 2011fe spectrum (Brown et al. 2016). These count rate ratios are the ones shown in Figure 3.

We can confirm a trend of colors with the light-curve shape (stretch or  $\Delta M_{15}(B)$ , as also seen in Brown et al. 2010 and Foley et al. 2016), so we exclude the rapidly declining SNe 2005ke and 2011iv from this analysis to focus on the UV differences of SNe Ia with more normal light-curve shapes.

Figure 3 shows the count rate ratios (with the color-based reddening correction) plotted with respect to the host-galaxy mass and metallicity as reported by Pan et al. (2020). Linear fits are performed using the Python Markov Chain Monte Carlo (MCMC) Bayesian linear fitting algorithm LINMIX (Kelly 2007). This process is able to account for heteroscedastic errors in both the *x* and *y* components of the fit. The uncertainties in the host-galaxy parameters from Pan et al. (2020) are not symmetric. In Table 1 we report results using the positive error bars for both, though we have checked that our conclusions are unchanged if we use just the negative error bars. We execute the MCMC fit with 10,000 draws from the posterior distribution and  $K = 2$  Gaussians in the mixture model. We provide the mean slope and intercept from the fits as well as the standard deviation of both of these parameters in Table 1. Values are provided for our color-based extinction correction as well as the original estimates of host reddening in Pan et al. (2020). The mean slopes show a different trend than that seen by Pan et al. (2020), namely we see stronger trends in the near-UV *u* and *uvw1* filters than in the mid-UV *uvm2* filter. Nevertheless, a significant fraction of the draws from the

<sup>4</sup> [https://people.physics.tamu.edu/pbrown/SwiftSN/swift\\_sn.html](https://people.physics.tamu.edu/pbrown/SwiftSN/swift_sn.html)

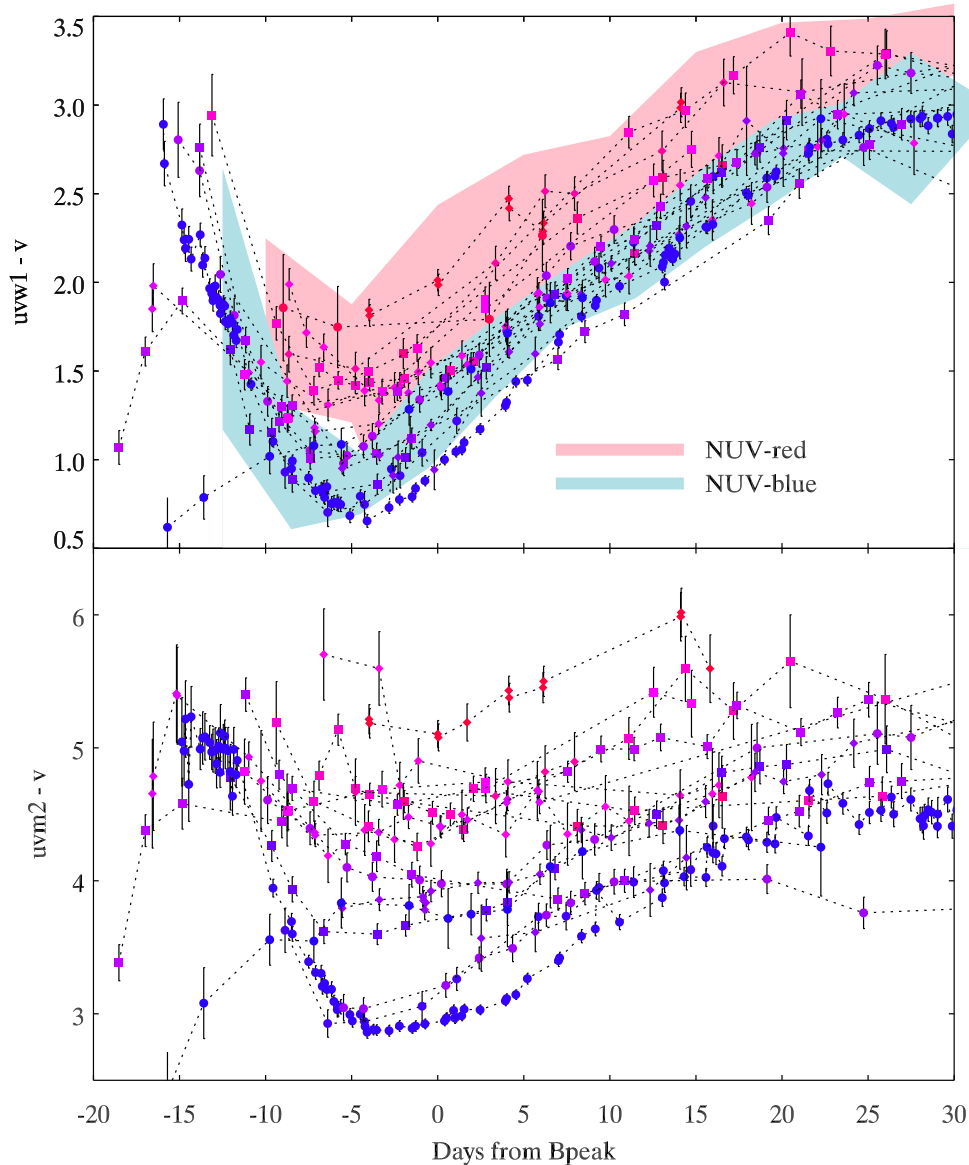


**Figure 1.**  $uvw1 - v$  and  $uvm2 - uvw1$  color evolution for the SNe Ia. This sample is identical to Pan et al. (2020) except for the exclusion of the rapidly declining SNe 2005ke and 2011iv and several SNe Ia that lack template images for host-galaxy flux subtraction. The colors of these SNe Ia cover a similar range to those studied previously by Milne et al. (2010) and Brown et al. (2017). The *Swift*/UVOT photometry gives a better view of the relative flux evolution than from the limited spectra available in Pan et al. (2020). Earlier than five days before *B*-band maximum light it is still hard to judge the spread in colors due to the faintness of most the objects in the mid-UV. A few objects, notably iPTF14bdn (Smitka et al. 2015) and SN 2017cbv (Hosseinzadeh et al. 2017), were bluer at earlier times than the majority of SNe Ia.

posterior distribution have positive and negative slopes, and the mean slope is never greater than one standard deviation of the sampled slopes. The limited number of SNe Ia with low host masses and low host-galaxy metallicities gives individual objects a disproportionate weight considering the large scatter in the more populated regions of the host-galaxy parameter space.

We also present the Kendall and Pearson correlation coefficients and  $p$ -values. These do not take into account the uncertainties, but are independent means of evaluating the significance of a correlation. The  $p$ -values are high, with the smallest being 0.16. Thus we do not find evidence with which to reject the null hypothesis that there is no correlation between the host-galaxy mass or metallicity and the UV-optical count rate ratios at the time of *B*-band maximum light.

#### 4. Discussion

The lack of correlations between the UV flux and the host-galaxy metallicity is surprising given the many models that predict strong UV effects. In particular, the lack of separation based on color in Figure 2 or correlation with metallicity in Figure 3 seems to contradict the conclusions of Brown et al. (2019) that the spectral differences between the NUV-blue SN 2011fe and the NUV-red SN 2017erp are related to the metallicity. Recent measurements of the gas-phase metallicity in two star-forming regions in NGC 5861 point to a subsolar metallicity ( $12 + \log(\text{OH}) = 7.67 \pm 0.01$  and  $7.87 \pm 0.03$ ; Muñoz-Vergara et al. 2019) for the host of the NUV-red SN 2017erp. These measurements would reinforce the observed lack of trend between host-galaxy metallicity and the UV colors of SNe Ia.

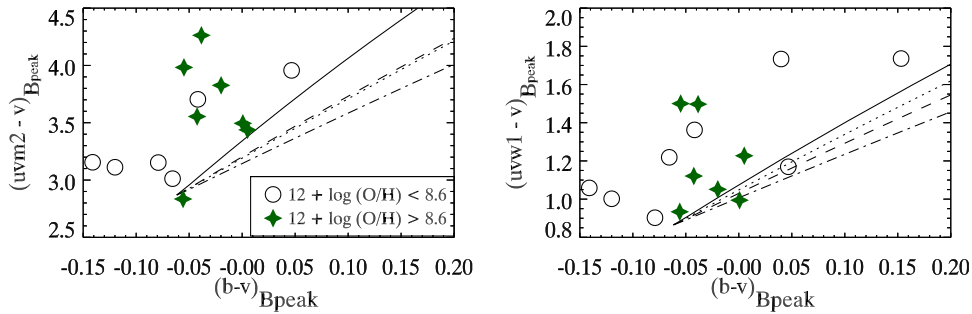


**Figure 2.** UV colors vs. optical colors observed at the time of maximum light in the  $B$  band. The lines represent the SN 2011fe spectrum reddened by different extinction laws (see Brown et al. 2017). The intrinsic dispersion is apparent from the vertical spread in points that is present for SNe Ia from low- and high-metallicity host galaxies.

There are a number of reasons that might contribute to a lack of correlation between the UV properties of the SNe Ia and the measured metallicities of their host galaxies. First, within a galaxy there are metallicity gradients (Zaritsky et al. 1994), such that the global gas-phase metallicity may not represent the gas-phase metallicity at the location of the SN progenitor. Galbany et al. (2016) found that on average there are small differences between the total and local metallicity. These differences were measured as  $-0.018$  and  $-0.088$  dex, respectively, for the oxygen and stellar metallicities. For the oxygen abundances, the metallicity measured at the location of individual objects changed from 0.1 below to 0.1 above that of the host galaxy as a whole, while the stellar metallicity differences ranged from  $-0.3$  to  $0.2$  dex. Zhou et al. (2019) used integral field spectroscopy to study the local, central, and global metallicities of SN hosts. They conclude that the bias is small between them, though individual objects varied by up to  $0.6$  dex. Though small, these metallicity differences within a galaxy are as large as the range of this sample of Pan et al. (2020). To give an example noted by Foley & Kirshner (2013), the metallicity of M101 measured by the Sloan Digital Sky Survey is  $9.12$  (Prieto et al. 2008), but the gradient results in a value of  $8.45$  at the location of SN 2011fe (Stoll et al. 2011, and see also Vilchez et al. 2019). The global versus local metallicity difference for SN 2011fe is as large as that between the lowest and highest metallicities of the galaxies in the sample of Pan et al. (2020). The lack of a correlation with the *global* host-galaxy metallicity does not rule out the possibility of a correlation with the *metallicity at the SN location*.

Second, the time between the birth of a star and when it eventually explodes leads to a difference between the progenitor metallicity and the gas-phase metallicity measured near the time and place of explosion due to the chemical evolution of the galaxy (Wyse & Silk 1987) and the migration of the progenitor from its birthplace. This depends on the delay time distribution between progenitor formation and explosion (see Bravo & Badenes 2011 and the discussion therein). SNe Ia in passive galaxies are found to have a larger difference than those in actively star-forming galaxies. If SNe Ia have the same delay from birth to explosion and the underlying host galaxies evolve in a uniform matter, then the metallicities would be uniformly shifted. Differences in the delay time and evolution of the galaxy metallicities, however, would lead to more scatter. The lack of a correlation with the *current* host-galaxy metallicity does not rule out the possibility of a correlation with the *progenitor metallicity at the time the progenitor formed*.

Third, the white dwarf progenitor may have a different composition at the time of explosion than it did at birth.

De et al. (2014) note that simmering causes a neutronization floor larger than that from the progenitor metallicity. They highlight that the most relevant parameter is the metallicity at the time of explosion. The lack of a correlation with the host-galaxy metallicity does not rule out the possibility of a correlation with the *SN progenitor metallicity at the time of explosion*.

Finally, the explosion itself results in a mixing of the products of nucleosynthesis that can mimic the effect of metallicity differences (Höflich et al. 1998). The models of Walker et al. (2012) acknowledge that the adopted composition structure could be affected by upmixing as well as primordial metallicity. The lack of an observed correlation with the host-galaxy metallicity does not rule out the possibility of a correlation with the *metal content in the SN ejecta*.

There are also complications of the observations and in the analysis that could mask a real correlation. While the UV photometry used here has much higher signal-to-noise ratio than the spectra used by Pan et al. (2020), we have a comparable (and slightly smaller) sample. This is particularly problematic in the regions of the low mass and low metallicity where single objects have an enhanced impact on the correlations. Even with this sample, however, it is clear that there is significant scatter beyond any possible correlation. Such a scatter points to other physics that is at least as important as progenitor metallicity to the formation and absorption of the UV flux. The next advances will require going beyond the existing models. Self-consistent modeling of the progenitor evolution, nucleosynthesis, radiative transfer, and computation of observables is needed (Bravo et al. 2010; Miles et al. 2016).

A further complication in UV analyses is the correction for dust reddening. In particular, if a relevant variable such as metallicity also affects the optical colors from which the reddening is estimated (Höflich et al. 2000; Walker et al. 2012; Brown et al. 2019), an inaccurate correction of the UV flux could enhance or diminish the physical effect being studied. Brown et al. (2018) showed this effect in a study of the UV colors of SNe Ia of differing velocities for which the effect of optical color is still being studied. This is important in studies such as this, because the amount and type of dust may also correlate with the host-galaxy properties.

## 5. Conclusions

In conclusion, we find no evidence for a correlation between the mass or metallicity and the UV–optical colors or count rate ratios. This in contrast to the findings of Pan et al. (2020), which we attribute to an overestimate of the UV flux for

**Table 1**  
MCMC Linear Fit Parameters

Host Parameter	Reddening Correction	Color Ratio	Slope	Intercept	Kendall Correlation Coefficient	Kendall <i>P</i> -value	Pearson Correlation Coefficient	Pearson <i>P</i> -value	% of Fits with Negative Slope
log(M)	P19	<i>u/b</i>	$0.03 \pm 0.03$	$0.39 \pm 0.28$	0.15	0.44	0.31	0.23	14
log(M)	P19	<i>w1/b</i>	$0.00 \pm 0.01$	$0.05 \pm 0.05$	0.16	0.44	0.19	0.50	36
log(M)	P19	<i>m2/b</i>	$-0.00 \pm 0.00$	$0.01 \pm 0.01$	-0.11	0.63	-0.05	0.87	70
12 + log(O/H)	P19	<i>u/b</i>	$0.23 \pm 0.26$	$-1.37 \pm 2.22$	0.15	0.51	0.39	0.19	16
12 + log(O/H)	P19	<i>w1/b</i>	$0.02 \pm 0.04$	$-0.11 \pm 0.37$	0.20	0.45	0.25	0.47	31
12 + log(O/H)	P19	<i>m2/b</i>	$0.00 \pm 0.01$	$-0.01 \pm 0.04$	0.16	0.54	0.39	0.24	36
log(M)	color	<i>u/b</i>	$0.03 \pm 0.03$	$0.45 \pm 0.30$	0.18	0.35	0.32	0.21	15
log(M)	color	<i>w1/b</i>	$0.00 \pm 0.01$	$0.05 \pm 0.05$	0.11	0.63	0.26	0.36	21
log(M)	color	<i>m2/b</i>	$-0.0 \pm 0.00$	$0.01 \pm 0.01$	0.05	0.85	0.05	0.86	58
12 + log(O/H)	color	<i>u/b</i>	$0.22 \pm 0.24$	$-1.18 \pm 2.08$	0.31	0.16	0.39	0.19	17
12 + log(O/H)	color	<i>w1/b</i>	$0.01 \pm 0.05$	$0.00 \pm 0.39$	0.13	0.65	0.18	0.60	42
12 + log(O/H)	color	<i>m2/b</i>	$0.00 \pm 0.01$	$-0.00 \pm 0.07$	0.09	0.76	0.41	0.22	51



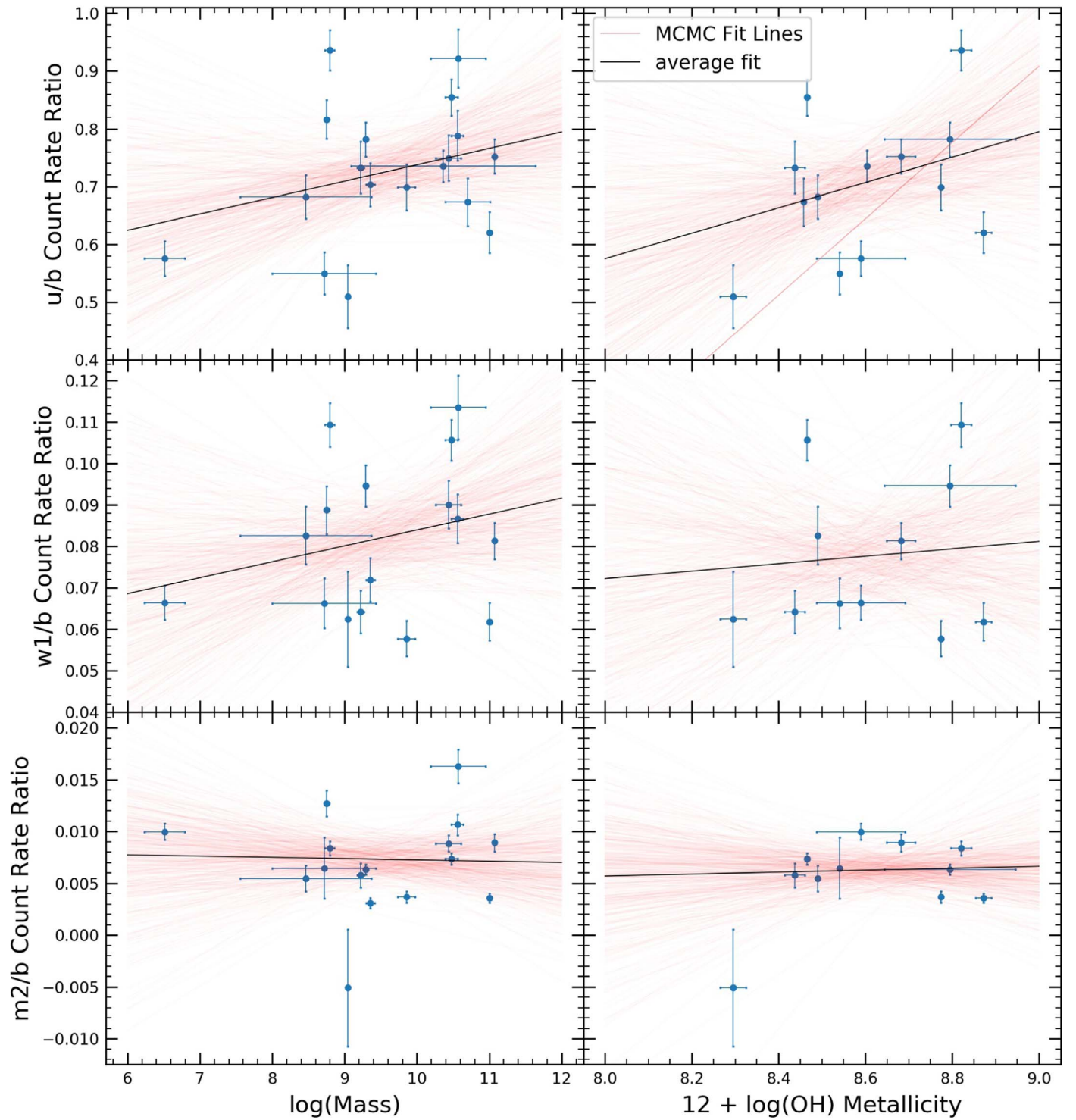


**Figure 3.** UV/optical count rate ratios of the SNe Ia compared to the mass and metallicity of the host galaxy. Based on the MCMC fit parameters displayed in Table 1, we do not find sufficient evidence for a correlation between the mass or metallicity of SN Ia host galaxies and the UV/optical count rate ratios from *Swift*/UVOT.

SN 2016ccz in the lowest-metallicity host galaxy of the sample. Samples covering a wider range in host-galaxy parameters will help elucidate any physical connections that may exist. The large scatter seen perpendicular to correlations of the UV flux with light-curve shape (Brown et al. 2010; Foley et al. 2016), optical colors (as a proxy for reddening; Brown et al. 2016), velocity (Milne et al. 2013; Brown et al. 2018),

and now host-galaxy mass and metallicity implies that yet another physical difference must exist between optically similar SNe Ia that strongly affects the UV. Further theoretical work is needed to compare against the multiwavelength and time-series data now available to better understand the diversity of these standard candles and how it might impact their use as cosmological distance indicators.

P.J.B. receives support through program #14665 provided by NASA through a grant from the Space Telescope Science Institute, which is operated by the Association of Universities for Research in Astronomy, Inc., under NASA contract NAS 5-26555. P.J.B. is also supported by the Mitchell Institute for Fundamental Physics and Astronomy at Texas A&M University. This work was supported by NSF grant AST-1560223 (PI: Marshall) “REU Site: Astronomical Research and Instrumentation at Texas A&M University.” We appreciate helpful comments from E. Baron, X. Yan, and N. Suntzeff.

*Facility:* *Swift* (UVOT).

*Software:* HEASOFT (NASA HEASARC 2014), CALDB, IDL Astronomy Library (Landsman 1993), astropy (Astropy Collaboration et al. 2013; Price-Whelan et al. 2018), scipy (Jones et al. 2001; Virtanen et al. 2019), linmix (Kelly 2007).

### ORCID iDs

Peter J. Brown  <https://orcid.org/0000-0001-6272-5507>

### References

- Astropy Collaboration, Robitaille, T. P., Tollerud, E. J., et al. 2013, *A&A*, **558**, A33
- Bravo, E., & Badenes, C. 2011, *MNRAS*, **414**, 1592
- Bravo, E., Domínguez, I., Badenes, C., Piersanti, L., & Straniero, O. 2010, *ApJL*, **711**, L66
- Brout, D., Scolnic, D., Kessler, R., et al. 2019, *ApJ*, **874**, 150
- Brown, P. J., Baron, E., Milne, P., Roming, P. W. A., & Wang, L. 2015, *ApJ*, **809**, 37
- Brown, P. J., Breeveld, A., Roming, P. W. A., & Siegel, M. 2016, *AJ*, **152**, 102
- Brown, P. J., Breeveld, A. A., Holland, S., Kuin, P., & Pritchard, T. 2014, *A&SS*, **354**, 89
- Brown, P. J., Hosseinzadeh, G., Jha, S. W., et al. 2019, *ApJ*, **877**, 152
- Brown, P. J., Landez, N. J., Milne, P. A., & Stritzinger, M. D. 2017, *ApJ*, **836**, 232
- Brown, P. J., Perry, J. M., Beeny, B. A., Milne, P. A., & Wang, X. 2018, *ApJ*, **867**, 56
- Brown, P. J., Roming, P. W. A., Milne, P., et al. 2010, *ApJ*, **721**, 1608
- Cardelli, J. A., Clayton, G. C., & Mathis, J. S. 1989, *ApJ*, **345**, 245
- Childress, M., Aldering, G., Antilogus, P., et al. 2013, *ApJ*, **770**, 108
- De, S., Timmes, F. X., Brown, E. F., et al. 2014, *ApJ*, **787**, 149
- Foley, R. J., & Kirshner, R. P. 2013, *ApJL*, **769**, L1
- Foley, R. J., Pan, Y.-C., Brown, P., et al. 2016, *MNRAS*, **461**, 1308
- Galbany, L., Stanishev, V., Mourão, A. M., et al. 2014, *A&A*, **572**, A38
- Galbany, L., Stanishev, V., Mourão, A. M., et al. 2016, *A&A*, **591**, A48
- Gehrels, N., Chincarini, G., Giommi, P., et al. 2004, *ApJ*, **611**, 1005
- Guillochon, J., Parrent, J., Kelley, L. Z., & Margutti, R. 2017, *ApJ*, **835**, 64
- Hamuy, M., Phillips, M. M., Suntzeff, N. B., et al. 1996, *AJ*, **112**, 2398
- Hayden, B. T., Gupta, R. R., Garnavich, P. M., et al. 2013, *ApJ*, **764**, 191
- Höflich, P., Nomoto, K., Umeda, H., & Wheeler, J. C. 2000, *ApJ*, **528**, 590
- Höflich, P., Wheeler, J. C., & Thielemann, F. K. 1998, *ApJ*, **495**, 617
- Hosseinzadeh, G., Sand, D. J., Valenti, S., et al. 2017, *ApJL*, **845**, L11
- Jones, E., Oliphant, T., Peterson, P., et al. 2001, SciPy: Open Source Scientific Tools for Python, <http://www.scipy.org/>
- Kelly, B. C. 2007, *ApJ*, **665**, 1489
- Kelly, P. L., Hicken, M., Burke, D. L., Mandel, K. S., & Kirshner, R. P. 2010, *ApJ*, **715**, 743
- Kim, A. G., Aldering, G., Antilogus, P., et al. 2014, *ApJ*, **784**, 51
- Kuin, N. P. M., Landsman, W., Breeveld, A. A., et al. 2015, *MNRAS*, **449**, 2514
- Lampeitl, H., Smith, M., Nichol, R. C., et al. 2010, *ApJ*, **722**, 566
- Landsman, W. B. 1993, in ASP Conf. Ser. 52, The IDL Astronomy User’s Library, ed. R. J. Hanisch, R. J. V. Brissenden, & J. Barnes (San Francisco, CA: ASP), 246
- Lentz, E. J., Baron, E., Branch, D., Hauschildt, P. H., & Nugent, P. E. 2000, *ApJ*, **530**, 966
- Mazzali, P. A., & Podsiadlowski, P. 2006, *MNRAS*, **369**, L19
- Miles, B. J., van Rossum, D. R., Townsley, D. M., et al. 2016, *ApJ*, **824**, 59
- Milne, P. A., Brown, P. J., Roming, P. W. A., Bufano, F., & Gehrels, N. 2013, *ApJ*, **779**, 23
- Milne, P. A., Brown, P. J., Roming, P. W. A., et al. 2010, *ApJ*, **721**, 1627
- Milne, P. A., Foley, R. J., Brown, P. J., & Narayan, G. 2015, *ApJ*, **803**, 20
- Moreno-Raya, M. E., Mollá, M., López-Sánchez, Á. R., et al. 2016, *ApJL*, **818**, L19
- Muñoz-Vergara, D., Firpo, V., Hägele, G. F., et al. 2019, *BAAA*, **61**, 207
- NASA HEASARC 2014, HEASoft: Unified Release of FTOOLS and XANADU, Astrophysics Source Code Library, ascl:1408.004
- Pan, Y.-C., Foley, R. J., Filippenko, A. V., & Kuin, N. P. M. 2018, *MNRAS*, **479**, 517
- Pan, Y. C., Foley, R. J., Jones, D. O., Filippenko, A. V., & Kuin, N. P. M. 2020, *MNRAS*, **491**, 5897
- Pettini, M., & Pagel, B. E. J. 2004, *MNRAS*, **348**, L59
- Phillips, M. M., Lira, P., Suntzeff, N. B., et al. 1999, *AJ*, **118**, 1766
- Price-Whelan, A. M., Sipőcz, B. M., Günther, H. M., et al. 2018, *AJ*, **156**, 123
- Prieto, J. L., Stanek, K. Z., & Beacom, J. F. 2008, *ApJ*, **673**, 999
- Riess, A. G., Press, W. H., & Kirshner, R. P. 1996, *ApJ*, **473**, 88
- Rigault, M., Copin, Y., Aldering, G., et al. 2013, *A&A*, **560**, A66
- Roming, P. W. A., Kennedy, T. E., Mason, K. O., et al. 2005, *SSRv*, **120**, 95
- Sauer, D. N., Mazzali, P. A., Blondin, S., et al. 2008, *MNRAS*, **391**, 1605
- Schlafly, E. F., & Finkbeiner, D. P. 2011, *ApJ*, **737**, 103
- Scolnic, D. M., Jones, D. O., Rest, A., et al. 2018, *ApJ*, **859**, 101
- Smitka, M. T., Brown, P. J., Kuin, P., & Suntzeff, N. B. 2016, *PASP*, **128**, 034501
- Smitka, M. T., Brown, P. J., Suntzeff, N. B., et al. 2015, *ApJ*, **813**, 30
- Stoll, R., Shappee, B., & Stanek, K. Z. 2011, *ATel*, **3588**, 1
- Timmes, F. X., Brown, E. F., & Truran, J. W. 2003, *ApJL*, **590**, L83
- Vílchez, J. M., Relaño, M., Kennicutt, R., et al. 2019, *MNRAS*, **483**, 4968
- Virtanen, P., Gommers, R., Oliphant, T. E., et al. 2019, arXiv:1907.10121
- Walker, E. S., Hachinger, S., Mazzali, P. A., et al. 2012, *MNRAS*, **427**, 103
- Wyse, R. F. G., & Silk, J. 1987, *ApJL*, **313**, L11
- Zaritsky, D., Kennicutt, R. C. J., & Huchra, J. P. 1994, *ApJ*, **420**, 87
- Zhou, L., Liang, Y. C., Ge, J. Q., et al. 2019, *RAA*, **19**, 121